Ramifications of increased salinity in tidal freshwater sediments: Geochemistry and microbial pathways of organic matter mineralization

Nathaniel B. Weston,[1,2] Ray E. Dixon,[1] and Samantha B. Joye[1]

Received 4 July 2005; revised 9 November 2005; accepted 13 December 2005; published 7 February 2006.

[1] The effects of salinity intrusion on the anaerobic microbial and geochemical dynamics of tidal freshwater sediments were investigated using flow-through sediment reactors. In freshwater control sediments, organic matter mineralization was dominated by methanogenesis (62%), followed by sulfate reduction (18%), denitrification (10%), and iron reduction (10%). Upon salinity intrusion, nutrient (ammonium, silicate, phosphate) concentrations increased and rates of methanogenesis declined. Iron-oxide bioavailability increased and microbial iron reduction appeared to account for >60% of organic matter oxidation for several days after salinity intrusion. However, sulfate reduction was the dominant pathway (>50%) of organic matter oxidation within 2 weeks of salinity intrusion, and accounted for >95% of total organic matter mineralization after 4 weeks. Total in situ sediment organic matter mineralization doubled following salinity intrusion. Increased nutrient release, decreased methanogenesis and a rapid shift to sulfate reduction, with a coincident increase overall organic matter mineralization, accompanied salinity intrusion into previously freshwater riverine sediments.

Citation: Weston, N. B., R. E. Dixon, and S. B. Joye (2006), Ramifications of increased salinity in tidal freshwater sediments: Geochemistry and microbial pathways of organic matter mineralization, *J. Geophys. Res.*, *111*, G01009, doi:10.1029/2005JG000071.

1. Introduction

[2] Climate change and freshwater withdrawal within the watersheds of rivers can reduce the volume of freshwater delivered by rivers to the coastal zone. As freshwater discharge decreases and the freshwater-saltwater mixing zone moves upriver, saline waters intrude into previously freshwater regions [*Hamilton*, 1990; *Knowles*, 2002]. Rising sea levels [*Wigley*, 2005], the potential for lower precipitation in watersheds of rivers [*Smith et al.*, 2005], and global increases in water consumption [*Gleick*, 2003] may result in widespread salinity intrusion in midlatitude coastal ecosystems in the near future. The increase in ionic strength and change in concentrations of substances during the transition from freshwater to saltwater conditions may exert a powerful influence on plant [*Crain et al.*, 2004], animal [*Kupschus and Tremain*, 2001], and microbial [*Rysgaard et al.*, 1999; *Mondrup*, 1999; *Dincer and Kargi*, 1999; *Pattnaik et al.*, 2000; *Mishra et al.*, 2003] community dynamics.

[3] Little is known about the microbial and geochemical ramifications of salinity increases in freshwater riverine sediments. Microbial methanogenesis [*Capone and Kiene*, 1988] and iron (Fe) reduction [*Roden and Wetzel*, 1996] dominate anaerobic organic matter mineralization in freshwater sediments. Methane (CH_4) is a powerful greenhouse gas, and freshwater wetlands are a major natural source of CH_4 to the atmosphere [*Wuebbles and Hayhoe*, 2002]. Owing to the greater availability of sulfate (SO_4^{2-}) in seawater, sulfate reduction replaces methanogenesis as the dominant anaerobic microbial terminal electron accepting process in marine sediments [*Jørgensen*, 1982; *Capone and Kiene*, 1988; *Howarth*, 1993].

[4] Salinity intrusion may also alter sediment microbial processes with repercussions for rates and patterns of nitrogen and phosphorus cycling. Primary production in freshwaters is generally limited by phosphorus [*Schindler*, 1977], while nitrogen limits production in marine waters [*Ryther and Dunstan*, 1971; *Nixon et al.*, 1996]. This shift in limiting nutrient from freshwater to marine environments is largely controlled by the anaerobic microbial processes occurring in sediments. Phosphorus (P) is coprecipitated with iron oxyhydroxides and thereby sequestered in sediments, creating P limitation of primary production in freshwater aquatic ecosystems. In marine sediments, hydrogen sulfide (HS^-) produced during sulfate reduction reacts abiotically with reactive iron oxyhydroxides, leading to reductive dissolution of iron minerals and the release of Fe-associated P. This P release results in greater P availability and, thus, nitrogen (N) limitation, of primary production in marine systems [*Caraco et al.*, 1989; *Harris*, 1999; *Blomqvist et al.*, 2004]. The pathways of anaerobic microbial metabolism thus influence the recycling, sequestration, and burial of carbon and nutrients on a global scale.

[1]Department of Marine Science, University of Georgia, Athens, Georgia, USA.
[2]Now at Patrick Center for Environmental Research, Academy of Natural Sciences, Philadelphia, Pennsylvania, USA.

0148-0227/06/2005JG000071$09.00

[5] Salinity intrusion into previously freshwater habitats is likely to have multiple profound affects on the microbial community and geochemistry of freshwater sediments, and may alter the fluxes of nutrients and greenhouse gasses from these environments. The shift from methanogenesis to sulfate reduction may reduce emissions of CH_4. However, nutrient fluxes may increase following salinity intrusion, influencing the magnitude of primary production in coastal waters. Little is known about the rate at which the freshwater sediment microbial community responds to changes in salinity driven by up-river salinity intrusion or how the geochemistry of the sediments is altered by salinity increases.

[6] In this study, we simulated and monitored the effects of salinity intrusion into anoxic sediments from the tidal freshwater portion of the Altamaha River, Georgia, using sediment flow-through reactors. Changes in concentrations of nutrients [ammonium (NH_4^+), nitrate+nitrite (NO_x), phosphate (HPO_4^{2-}), silicate (SiO_3^{2-})], SO_4^{2-}, dissolved organic carbon and nitrogen (DOC and DON, respectively), major ions [chloride (Cl^-), sodium (Na^+), potassium (K^+), magnesium (Mg^{2+}), calcium (Ca^{2+})], reduced iron (Fe^{2+}) and manganese (Mn^{2+}), CH_4, nitrous oxide (N_2O), HS^- and dissolved inorganic carbon (DIC) and pH of water flowing through the reactors was measured during, and for several weeks after, salinity intrusion and in freshwater controls. Sediment solid-phase C, N, P, S and Fe concentrations were determined at several time points during the experiment. Rates of microbial organic matter mineralization coupled to sulfate reduction, methanogenesis, iron reduction and denitrification in freshwater sediments were calculated, and the shifts in these pathways following salinity intrusion were determined.

2. Methods

2.1. Study Site

[7] The Altamaha River drains the third largest watershed on the East coast of the United States (approximately 36,000 km^2). The watershed lies entirely within the state of Georgia, and watershed land use is a mixture of pristine, agricultural and residential/urban. The watershed remains relatively undeveloped compared with other East coast watersheds, although development pressure is increasing (N. B. Weston et al., Thirty years of land use change in the Altamaha River watershed and the impacts on nutrient loading in the Altamaha River, submitted to *Water Research*, 2005) (hereinafter referred to as Weston et al., submitted manuscript, 2005). Inorganic nitrogen concentrations have increased from the 1970s through 2000, largely owing to residential and urban development in the upper portions of the watershed near metropolitan Atlanta. NO_3^- concentrations average about 20 μM (Weston et al., submitted manuscript, 2005). Discharge from the Altamaha River averages about 400 $m^3\ s^{-1}$, but has declined by 4.2 $m^3\ s^{-1}$ per year over the past 3 decades (Weston et al., submitted manuscript, 2005). Although water-withdrawal within the watershed has increased since 1950 [*Fanning*, 2003], lower river discharge is attributed to long-term climate change as precipitation within the watershed has also significantly decreased (Weston et al., submitted manuscript, 2005).

[8] Sediments from the tidal freshwater portion of the Altamaha River were sampled on July 12, 2004. Intact sediment cores (8.8 cm inner diameter) were obtained from the unvegetated, intertidal creek bank at low tide. Cores were transported to the laboratory, stored at in situ temperatures overnight, and sectioned for pore water and solid-phase sampling and for flow-through bioreactor experiments the following day.

2.2. Pore Water Profiles

[9] Duplicate sediment cores were sectioned under a nitrogen gas atmosphere (1 cm intervals to 4 cm, and 2 cm intervals to 20 cm) for pore water and solid-phase analyses. Sediment was centrifuged to obtain pore water, which was split into several vials for analysis of NH_4^+, NO_x, HPO_4^{2-}, SiO_3^{2-}, SO_4^{2-}, DOC, DON, Cl^-, Na^+, K^+, Mg^{2+}, Ca^{2+}, Fe^{2+}, HS^-, DIC and pH (Table 1). CH_4 and N_2O concentrations were determined by subsampling 2 cm^{-3} of sediment from intact cores directly into a helium-purged headspace vial containing 2 mL of 1 N NaOH which was immediately sealed and mixed. A known volume of sediment from each depth was dried (80°C) to determine porosity and bulk density; the samples were stored for subsequent solid-phase analysis of sediment carbonate, total carbon (C), nitrogen (N), and sulfur (S), exchangeable NH_4^+ (X-NH_4^+) and phosphorus (P) and iron (Fe) fractions (Table 1).

2.3. Flow-Through Reactors

[10] Sediment flow-through bioreactor experiments [*Roychoudhury et al.*, 1998, 2003; *Brüchert and Arnosti*, 2003] were initiated one day after sampling. Sediment from the 3- to 5-cm depth of 12 intact sediment cores was extruded into twelve separate flow-through reactors (8.8 cm inner diameter). This sediment depth was chosen as it was likely an active zone of anaerobic microbial organic matter processing. Sediment flow-through reactors were constructed of polycarbonate plastic and consisted of a 2-cm section of sediment, capped on either end with a 15-μm frit and held in place with an upper and lower housing. The polycarbonate housings had an inlet/outlet in the center, and spiral grooves on the inner surface to promote diffuse flow across the surface of the frit. The assembly was bolted lightly together and sealed with viton O-rings between the core, frit and housing.

[11] The sediment flow-through reactors, along with a peristaltic pump, inflow reservoirs and all tubing were placed in an anoxic Coy® chamber under a nitrogen gas atmosphere. Artificial freshwater (AFW, Table 2), purged of oxygen using nitrogen gas and kept anoxic in the Coy chamber, was pumped from the inflow reservoir through all of the reactors at a slow flow rate ($\sim$10 mL hr^{-1}). Pore water in the reactors was replaced approximately twice a day at this flow rate. The absence of oxygen in the inflow reservoirs was verified using an oxygen microelectrode (Unisense®). The AFW chemistry was based on average Altamaha River chemistry as measured by the Georgia Coastal Ecosystem Long Term Ecological Research project (http://gce-lter.marsci.uga.edu/lter/).

[12] After a 5-day equilibration and pore water flushing period in which all 12 reactors received AFW, the salinity of the inflow water was gradually increased in

Table 1. Sampling, Preservation, and Analytical Methods for Aqueous and Solid-Phase Sediment Samples From Initial Sediment Cores and Flow-Through Reactors[a]

Analyte	Sample	Preservation	Analytical Method
		Pore Water and Flow-Through Reactor Aqueous Analyses	
CH_4	unfiltered in He purged vial	4.4 N phosphoric acid	Shimadzu GC 14A flame ionization detector gas chromatograph
DIC	unfiltered	run immediately	Shimadzu TOC 5000 infra-red gas analyzer
pH	unfiltered	run immediately	Accumet AP62 pH meter and Sensorex 450C pH probe
HS^-	unfiltered	0.1 M zinc acetate	Colorimetric [*Cline*, 1969]
Cl^-, SO_4^{2-}, Na^+, K^+, Mg^{2+}, Ca^{2+}	0.2 μm filtered	0.2 N nitric acid	Dionex ion chromatograph
Fe^{2+}	0.2 μm filtered	0.2 N nitric acid	Colorimetric [*Stookey*, 1970]
Mn^{2+}	0.2 μm filtered	0.2 N nitric acid	Colorimetric [*Armstrong*, 1979]
HPO_4^{2-}	0.2 μm filtered	0.2 N nitric acid	Lachat Quikchem 8000 autoanalyzer (method 31-115-01-1G)
DOC	0.2 μm filtered	0.2 N nitric acid	Shimadzu TOC 5000 high-temperature combustion infra-red gas analyzer after sparging with CO_2-free air
NO_x (NO_3^- + NO_2^-)	0.2 μm filtered	refrigerated	Antek Instruments model 745 vanadium reduction manifold and model 7050 nitric oxide detector
DON	0.2 μm filtered	refrigerated	Shimadzu TOC 5000 and Antek 7020 nitric oxide detection for total dissolved nitrogen (TDN). DON = TDN − NH4+ − NOx
SiO_3^{2-}	0.2 μm filtered	refrigerated	Lachat Quikchem 8000 autoanalyzer (method 31-114-27-1-B)
NH_4^+	0.2 μm filtered	0.4% phenol	Colorimetric [*Solorzano*, 1969]
		Sediment Solid-Phase Analyses	
Porosity, bulk density	sediment	dried (80°C)	drying known volume of sediment
C, N, S	sediment	dried and ground	ThermoFinnigan Flash EA 1112 CNS Analyzer
Carbonate	sediment	dried and ground	in-line acidification on Shimadzu TOC-5000
P	sediment	frozen (−80°C)	SEDEX sequential extraction [*Ruttenberg*, 1992]
Reactive Fe	sediment	frozen (−80°C)	sequential extraction [*Poulton and Canfield*, 2005]
X-NH_4^+	sediment	frozen (−80°C)	sequential NaCl extraction; 0.145 M (10‰), 0.55 M (35‰), and 2 N (total)

[a]Methane (CH_4), dissolved inorganic carbon (DIC), hydrogen sulfide (HS^-), chloride (Cl^-), sulfate (SO_4^{2-}), sodium (Na^+), potassium (K^+), magnesium (Mg^{2+}), calcium (Ca^{2+}), reduced iron (Fe^{2+}), reduced manganese (Mn^{2+}), phosphate (HPO_4^{2-}), dissolved organic carbon (DOC), nitrate (NO_3^-), nitrite (NO_2^-), dissolved organic nitrogen (DON), silicate (SiO_3^{2-}), ammonium (NH_4^+), sediment carbon (C), nitrogen (N), sulfur (S), phosphorus (P), iron (Fe), and exchangeable ammonium (X-NH_4^+).

six of the reactors. Artificial seawater (ASW, based on average seawater chemistry) was mixed with AFW (Table 2) in increasing ratios to generate a 10‰ increase in salinity over a 2-week period. Salinity was then held constant at 10‰ for three additional weeks. The final salinity of 10‰ represents an increase to about one-third strength seawater, a reasonable but significant increase in salinity. Control reactors received AFW for the duration of the experiment. Duplicate reactors from both the control and salinity treatments were sacrificed for sediment solid-phase measurements on days 9 and 15 and upon termination of the experiment (day 35). Reactors were disassembled and a known volume of sediment was dried (80°C) for porosity and bulk density determinations and stored for later sediment solid-phase analysis of carbonate, C, N, S, X-NH_4^+ and P and Fe fractions (Table 1).

[13] Water exiting the flow-through reactors was sampled daily (through day 18) or every few days (after day 18) for NH_4^+, NO_x, HPO_4^{2-}, SiO_3^{2-}, SO_4^{2-}, DOC, DON, Cl^-, Na^+, K^+, Mg^{2+}, Ca^{2+}, Fe^{2+}, Mn^{2+}, HS^-, CH_4, N_2O, DIC and pH (Table 1). Outflow tubing was placed in a 20-mL glass vial, which was allowed to fill and overflow for several volumes before subsampling for the various analyses (Table 1). The inflow reservoirs were also sampled throughout the experiment, and there was no significant deviation from expected concentrations. The flow rate through the reactors was monitored for the duration of the experiment by measuring the

Table 2. Composition of Artificial Fresh Water (AFW) and Artificial Seawater (ASW) Flow-Through Reactor Inflow Solutions[a]

Component	AFW	ASW
Salinity, ‰	0.063	9.9
pH	7.9	7.9
Dextran, μM C	200	200
	Major Ions	
Cl^-, μM	980	155,132
Na^+, μM	910	148,794
Mg^{2+}, μM	98	7169
Ca^{2+}, μM	323	2897
K^+, μM	87	2813
SO_4^{2-}, μM	35	7969
HCO_3^-, μM	669	669
	Nutrients	
NH_4^+, μM	0.94	0.94
HPO_4^{2-}, μM	0.15	0.15
NO_3^-, μM	19.78	0.20

[a]Artificial fresh water, AFW; artificial seawater, ASW.

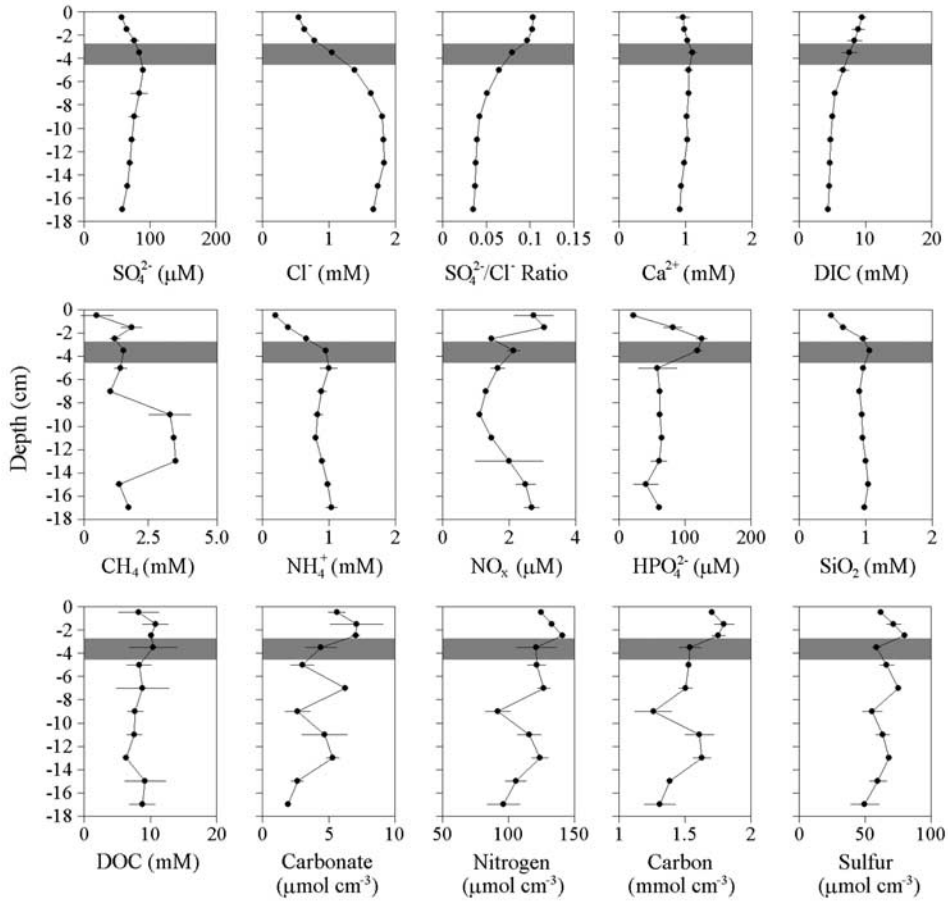

Figure 1. Average (± standard deviation, n = 2) porewater sulfate (SO_4^{2-}), chloride (Cl^-), sulfate to chloride ratio (SO_4^{2-}/Cl^-), calcium (Ca^{2+}), dissolved inorganic carbon (DIC), methane (CH_4), ammonium (NH_4^+), nitrate+nitrite (NO_x), phosphate (HPO_4^{2-}), silicate (SiO_3^{2-}), and dissolved organic carbon (DOC) and sediment solid-phase carbonate, organic nitrogen, organic carbon, and total sulfur. The depth of sediment used in the flow-through reactor experiments (3–5 cm) is indicated by the shaded area.

volume exiting each reactor over a known period of time.

3. Results

3.1. Pore Water Profiles

[14] Pore water Cl^- concentrations in the Altamaha River sediments increased slightly with depth, from about 0.5 at the surface to 1.5 mM at 2 cm (Figure 1). SO_4^{2-} concentrations increased with depth until 5 cm, and then decreased to about 50 μM (Figure 1). SO_4^{2-}/Cl^- molar ratios decreased in the 3 to 10 cm depth range from 0.1 in the surface sediments to 0.04 in deeper sediments. Ca^{2+} and DIC concentrations decreased with depth, while NH_4^+ and SiO_3^{2-} increased with depth (Figure 1). HPO_4^{2-} and NH_4^+ concentrations were relatively constant below 5 cm, but exhibited shallow (3–5 cm) concentration maxima (Figure 1). NO_x concentrations decreased with depth until 9 cm, below which NO_x increased slightly. Inorganic nitrogen was dominated by NH_4^+ (~0.8 mM), as pore water NO_x concentrations were low (~2 μM). CH_4 concentrations were above 1 mM except in the surface sediment, and DOC concentrations exceeded 5 mM (Figure 1).

3.2. Flow-Through Reactors

[15] Increased concentrations of major ions (Na^+, SO_4^{2-} (Figure 2); Cl^-, K^+, Mg^{2+}, Ca^{2+} (data not shown)) were observed in salinity-amended reactors. Differences in major ion concentration exiting the control and salinity-amended reactors were small but significant ($p < 0.001$) on the day following initiation of salinity increase. Major ion concentrations increased smoothly until day 15 (day number denotes days after start of the salinity-amendment), and were then constant until the termination of the experiment (Figure 2). SO_4^{2-} consumption during the salinity ramp was estimated using Na^+ concentrations to calculate an expected SO_4^{2-} [$(SO_4^{2-})_E$] concentration, assuming that Na^+ was unreactive,

$$\left(SO_4^{2-}\right)_E = \left[\left(Na^+ - Na^+_{AFW}\right)/\left(Na^+_{ASW} - Na^+_{AFW}\right)\right] * \left(SO_4^{2-}{}_{ASW} - SO_4^{2-}{}_{AFW}\right) + SO_4^{2-}{}_{AFW}, \quad (1)$$

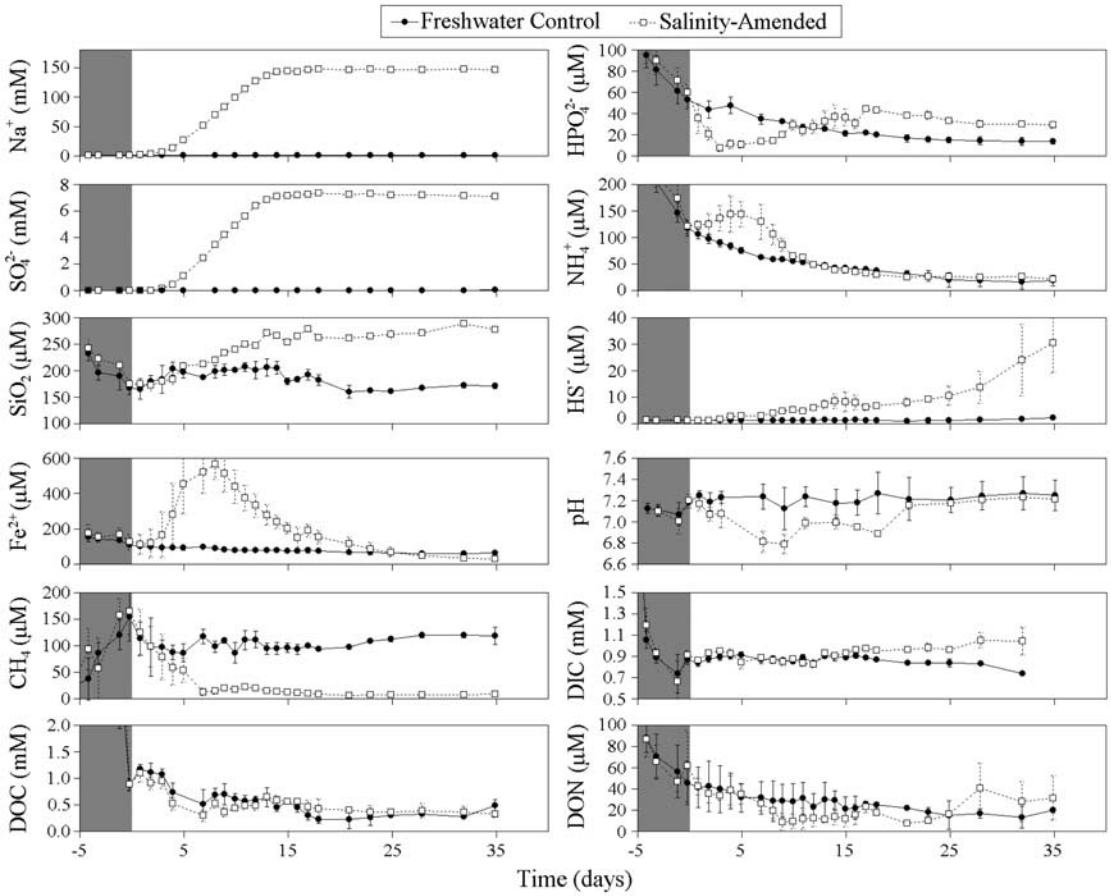

Figure 2. Concentrations (mean ± standard deviation; n = 6 for day −5 to day 8; n = 4 for day 9 to day 16; n = 2 for day 17 to day 35) of sodium (Na^+), sulfate (SO_4^{2-}), silicate (SiO_3^{2-}), reduced iron (Fe^{2+}), methane (CH_4), dissolved organic carbon (DOC), phosphate (HPO_4^{2-}), ammonium (NH_4^+), hydrogen sulfide (HS^-), dissolved inorganic carbon (DIC), pH, and dissolved organic nitrogen (DON) of water exiting control and salinity-amended flow-through reactors. The shaded area denotes the pre-equilibration period.

where Na^+, Na^+_{AFW} and Na^+_{ASW} are the measured, AFW and ASW sodium concentrations, respectively, and $SO_4^{2-}{}_{AFW}$ and $SO_4^{2-}{}_{ASW}$ are the AFW and ASW sulfate concentrations, respectively. The change in sulfate concentration reflecting consumption via sulfate reduction (ΔSO_4^{2-}) was then calculated by subtracting the measured SO_4^{2-} from $(SO_4^{2-})_E$. Net sulfate consumption occurred in both the control and salinity-amended reactors (Figure 3). ΔSO_4^{2-} averaged about 25 μM in control reactors for the entire experiment, while consumption rates in salinity-amended flow-through reactors increased rapidly as SO_4^{2-} concentrations increased during the salinity ramp (Figure 3). ΔSO_4^{2-} decreased to levels equivalent to those in the freshwater controls on day 9, and then increased, reaching about 300 μM by the termination of the experiment (Figure 3).

[16] A number of significant ($p < 0.05$) persistent (SiO_3^{2-}, CH_4, DIC, HS^-) or transient (Fe^{2+}, HPO_4^{2-}, NH_4^+, pH) differences in the concentration of dissolved species exiting control and salinity-amended flow-through reactors were observed during the experiment (Figure 2). Concentrations of SiO_3^{2-} exiting the control reactors dropped slightly during the experiment, but remained between 150 and 200 μM after the initial flushing of pore water (Figure 2). SiO_3^{2-} concentrations in salinity-amended reactors increased above control concentrations ($p < 0.05$) on day 7 and remained elevated (>250 μM) for the duration of the experiment (Figure 2). CH_4 concentrations decreased in salinity-amended reactors, becoming significantly lower than control reactor concentrations on day 5 ($p < 0.01$). CH_4 concentration in the control reactors was relatively constant at about 100 μM, while CH_4 concentrations remained below 20 μM after day 7 in salinity-amended reactors (Figure 2).

[17] DIC concentrations were similar in the control and salinity-amended reactors until day 15, after which DIC concentrations in salinity-amended reactors were significantly higher ($p < 0.05$, Figure 2). Net DIC production (ΔDIC, which reflects correction for inflow DIC concentrations) was relatively constant in control reactors, averaging about 150 μM (Figure 3). Net DIC production in salinity-amended reactors paralleled that of control reactors until day 15, after which DIC production increased to a maximum of about 400 μM (Figure 3). HS^- concentration

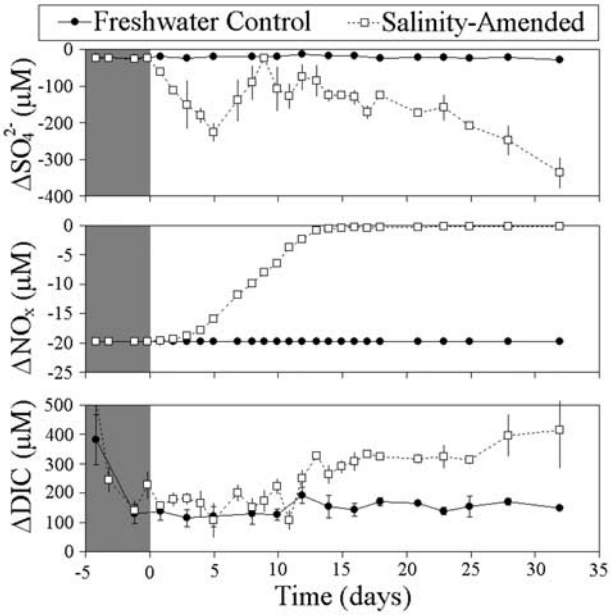

Figure 3. Net change in concentrations (± standard deviation, see text for description; n = 6 for day −5 to day 8; n = 4 for day 9 to day 16; n = 2 for day 17 to day 35) of sulfate (ΔSO_4^{2-}), nitrate+nitrite (ΔNO_x), and dissolved inorganic carbon (ΔDIC) during flow through control and salinity-amended sediment reactors.

in salinity-amended reactors increased above those in control reactors on day 4 ($p < 0.05$), reaching concentrations of about 30 μM by the end of the experiment.

[18] Fe^{2+} and NH_4^+ concentrations increased during the salinity ramp, and then decreased to match levels in the control reactors shortly after the salinity stabilized at 10‰. Fe^{2+} was significantly ($p < 0.05$) higher in salinity-amended reactors from day 3 until day 16, and peak concentrations exceeded 500 μM (days 7–9, Figure 2). NH_4^+ concentrations in salinity-amended reactors exceeded those in the control reactors on day 1 of the salinity ramp and remained significantly higher through day 11 ($p < 0.05$, Figure 2). HPO_4^{2-} concentrations initially decreased in salinity-amended reactors, becoming significantly lower than control concentrations on day 2, and remaining lower through day 9 ($p < 0.05$, Figure 2). HPO_4^{2-} concentrations then increased in salinity-amended reactors, becoming significantly higher than concentrations exiting control reactors on day 15 ($p < 0.05$, Figure 2). The pH in salinity-amended reactors decreased during the salinity ramp, becoming significantly different from control reactors on day 1 and remaining significantly lower (by about 0.4 pH units at peak difference) through day 18 ($p < 0.05$, Figure 2). The increase in Fe^{2+} exiting the reactors occurred during the period of decreased pH (Figure 2). The pH and $\log[Fe^{2+}]$ were significantly ($p < 0.001$) correlated, and the slope ($\log[Fe^{2+}] = -2.19$ pH) was similar to the stability isopleths of goethite and amorphous $Fe(OH)_3$ (Figure 4), in which $\log[Fe^{2+}] = 3$ pH [*Stumm and Morgan*, 1996].

[19] NO_x and Mn^{2+} concentrations were below detection in the effluent from both freshwater control and salinity-amended reactors for the duration of the experiment (data not shown). The change in NO_x concentration during flow through the sediment reactors (ΔNO_x; Figure 3) was calculated from the concentration of NO_x in inflow water. NO_x consumption was thus 20 μM in the control reactors, and decreased with decreasing NO_x in the inflow water to 0.2 μM in the salinity-amended reactors (Figure 3). No significant differences in concentrations of DOC or DON were observed between control and salinity-amended reactors (Figure 2).

[20] Total export (μmol cm^{-3}) of NH_4^+, HPO_4^{2-}, SiO_3^{2-}, Fe^{2+}, CH_4, and total carbon ($\sum C$, which equals the sum of DIC and CH_4 production, see below) and in situ $\sum C$ (in situ $\sum C$ = C derived from in situ organic matter mineralization and was estimated by correcting the $\sum C$ for the added dextran) for control and salinity-amended reactors was determined for the 35 days following the initial equilibration period (Table 3). Nutrient (NH_4^+, HPO_4^{2-} and

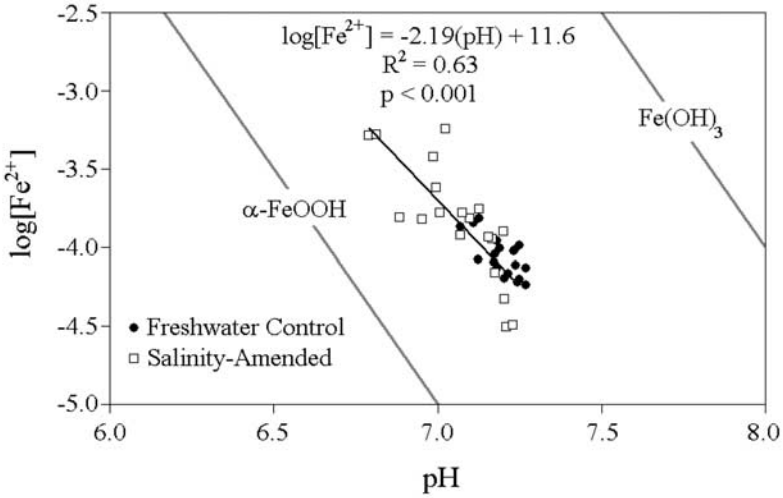

Figure 4. Diagram of pH and $\log[Fe^{2+}]$ concentrations of water exiting control and salinity-amended flow-through reactors. The stability isopleths for goethite (FeOOH) and amorphous iron oxides [$Fe(OH)_3$] are indicated.

Table 3. Total Export From Freshwater and Salinity-Amended Sediment Flow-Through Reactors of Ammonium, Phosphate, Silicate, Reduced Iron, Methane, Total Inorganic Carbon, and in Situ Carbon From the Altamaha River, and the Percent Change Due to Salinity Intrusion[a]

	Freshwater	Salinity Intrusion	Percent Change
NH_4^+	2.84	3.71	30.7
HPO_4^{2-}	1.58	1.90	20.7
SiO_3^{2-}	11.54	15.96	38.3
Fe^{2+}	4.86	12.08	148.6
CH_4	6.93	1.61	−76.8
$\sum C$	16.21	20.29	25.2
In situ C	3.72	7.80	109.7

[a]Export is in μmol cm^{-3} and denotes outflow minus inflow integrated over 35 days. Ammonium, NH_4^+; phosphate, HPO_4^{2-}; silicate, SiO_3^{2-}; reduced iron, Fe^{2+}; methane, CH_4; total inorganic carbon, $\sum C$; in situ carbon, in situ C. $\sum C$ is the total carbon (DIC and CH_4) production, and in situ C is $\sum C$ corrected for carbon (dextran) addition (12.5 μmol cm^{-3}).

SiO_3^{2-}) export from salinity-amended reactors was between 20% and 40% higher than that from control reactors (Table 3). Fe^{2+} export from salinity-amended reactors increased by 150%, while CH_4 export decreased by 75%. $\sum C$ export was 25% higher from salinity-amended reactors but, when corrected for dextran additions, in situ $\sum C$ export more than doubled (Table 3).

3.3. Solid Phase

[21] Sediment carbonate, organic nitrogen, organic carbon and total sulfur all significantly decreased with depth in the sediment cores ($p < 0.05$), and the C:N ratio was constant with depth (Figure 1). Carbonate content of the sediment was low (< 0.01% by weight), and organic carbon was several orders of magnitude higher (about 5% by weight, Figure 1). The measured carbonate may have reflected the DIC in solution when the sediment was dried, as the concentrations are similar and the sediment was not rinsed before carbonate analysis. Sediment organic nitrogen was also about 2 orders of magnitude higher than pore water inorganic nitrogen (Figure 1).

[22] Sediment total P was dominated largely by organic P, and the inorganic P fractions (adsorbed, acetate, and HCl extractable) accounted for only about 20% of the total (Table 4). The inorganic P was composed mainly of HCl extractable phases; Fe bound P accounted for only 5% of total P (Table 4). Dithionite-reducible Fe [*Poulton and Canfield*, 2005] was relatively high and accounted for about half of the total Fe (Table 4). Adsorbed Fe (i.e., 1 M $MgCl_2$ extractable [*Poulton and Canfield*, 2005]) was low and did not change during the experiment (Table 4).

[23] There were no detectable changes in sediment solid phase organic carbon, organic nitrogen, total sulfur or P fractions during the experiment (Table 4). Reducible Fe content in salinity-amended sediments at the end of the experiment (51.6 μmol cm^{-3}) was significantly ($p < 0.05$) lower than that measured in control reactors or initial sediments (Table 4). Other fractions of Fe did not change during the experiment.

[24] The 10‰-, 35‰-, 2N- and total-exchangeable NH_4^+ were all significantly lower ($p < 0.05$) in the control and salinity-amended reactors on days 9, 15 and 35 than in the initial Altamaha River sediments (Table 4, Figure 5). 10‰- and total-exchangeable NH_4^+ were higher in the control sediments than in the salinity-amended sediments at all time points, as was 35‰-exchangeable NH_4^+ on days 9 and 15 (Figure 5). Total-exchangeable NH_4^+ was dominated by 10‰-exchangeable (∼70%) in the initial and control sediments, but 10‰-exchangeable NH_4^+ accounted for only 30% of the total-exchangeable NH_4^+ in the salinity-amended reactors by day 35 (Figure 5). There were no significant differences in sediment 2N-exchangeable NH_4^+ content between the control and salinity-amended reactors (Figure 5).

3.4. Microbial Processes

[25] Rates of metabolic pathways in the flow-through reactors were estimated using a simple model of C production, on a per mole carbon basis,

$$\sum C = DNF + FeR + SR + MG, \quad (2)$$

Table 4. Sediment Solid-Phase Measurements (mean ± standard deviation) From Initial Core (3–5 cm depths, n = 2) and Control and Salinity-Amended Flow-Through Reactors Sampled at the End of the Experiment[a] (day 35, n = 2 each)[a]

Solid Phase Measurement	Initial	Control	Salinity
Carbonate	3.72 ± 0.15	3.83 ± 1.17	3.54 ± 0.15
Organic Nitrogen	121.2 ± 4.2	122.1 ± 8.7	112.8 ± 7.5
Organic Carbon	1534 ± 37	1584 ± 76	1603 ± 88
Total Sulfur	62.5 ± 1.0	74.1 ± 8.6	71.7 ± 7.2
Ammonium			
10‰ exchangeable	1.262 ± 0.284	**0.397** ± 0.075, I,S	**0.073** ± 0.002, I,S
32‰ exchangeable	0.369 ± 0.036	**0.113** ± 0.032, I	**0.097** ± 0.006, I
2N exchangeable	0.137 ± 0.010	**0.076** ± 0.017, I	**0.096** ± 0.011, I
Total exchangeable	1.77 ± 0.33	**0.59** ± 0.11, I,S	**0.27** ± 0.02, I,S
Phosphorus			
Exchangeable	0.035 ± 0.008	0.023 ± 0.010	0.063 ± 0.046
Authigenic apatite	0.81 ± 0.06	0.75 ± 0.05	0.70 ± 0.03
Total inorganic	2.31 ± 0.07	2.24 ± 0.10	2.35 ± 0.22
Organic	11.89 ± 1.47	11.74 ± 2.35	8.68 ± 1.45
Total	14.2 ± 1.4	14.0 ± 2.2	11.0 ± 1.2
Iron			
Exchangeable	0.33 ± 0.26	0.26 ± 0.11	0.52 ± 0.30
Reducible Fe(III)-oxides	61.8 ± 1.7	**71.0** ± 6.4, S	**51.6** ± 1.8, I,S
Total	115.6 ± 5.2	121.4 ± 18.7	112.4 ± 10.7

[a]Sediment solid-phase measurements are mean ± standard deviation. Initial core is 3- to 5-cm depths, n = 2. End of the experiment is day 35, n = 2 each. All units are in μmol (of C, N, S, P, or Fe) cm^{-3} of wet sediment. Statistical differences, in boldface ($p < 0.05$, pair wise), between reactors and initial sediment (I) and between control and salinity-amended reactors (S) are noted.

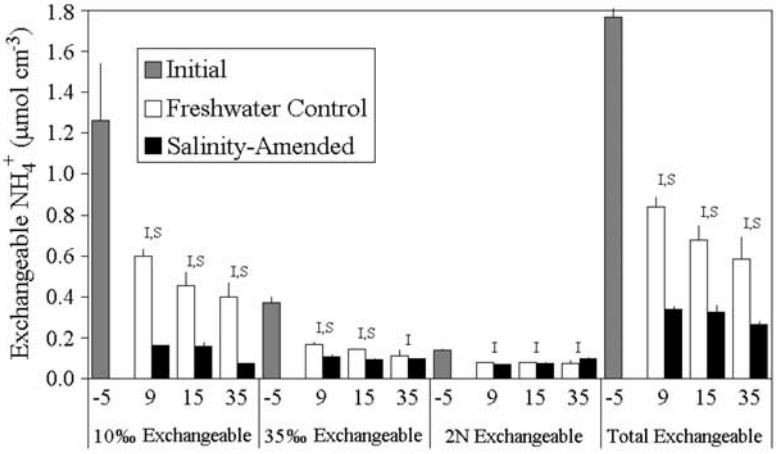

Figure 5. The 10‰, 35‰, 2N, and total exchangeable NH_4^+ from initial sediment cores (3- to 5-cm depth) and control and salinity-amended flow through reactors sampled on days 9, 15, and 35 (mean ± standard deviation, n = 2). Statistical differences ($p < 0.05$, pair wise) between reactors and initial sediment (I) and between control and salinity-amended reactors (S) are noted.

where $\sum$C is the total carbon production (DIC plus CH_4) and DNF, FeR, SR and MG are estimated rates of microbial denitrification, iron reduction, sulfate reduction and methanogenesis, respectively. Net rates (nmol cm^{-3} d^{-1}) of CH_4 and Fe^{2+} production (Figure 2) and NO_x and SO_4^{2-} consumption (Figure 3) were calculated from changes in concentration (Figures 2 and 3, Table 4) and the flow rate (10 mL hr^{-1}) through the reactors. DIC production via FeR, DNF and SR were estimated from Fe^{2+} production and NO_3^- and SO_4^{2-} consumption using ratios of 0.25, 1.125 and 2 DIC produced per Fe^{2+} produced and NO_3^- and SO_4^{2-} consumed, respectively [*Stumm and Morgan*, 1996]. MG was estimated using the following equation:

$$MG = (2f)\Delta CH_4 + (1 - f)\Delta CH_4, \quad (3)$$

where f is the fraction of CH_4 produced (ΔCH_4) from organic matter (i.e., acetoclastic methanogenesis, MG_A),

MG_A

$$CH_3COOH \rightarrow CO_2 + CH_4, \quad (4)$$

and the remaining CH_4 (1 − f) is produced via hydrogenotrophic methanogenesis (MG_H),

MG_H

$$CO_2 + H_2 \rightarrow CH_4 + 2H_2O. \quad (5)$$

The terminal carbon produced via MG_A reflects both the CH_4 and CO_2 produced

$$MG_A = 2f(\Delta CH_4), \quad (6)$$

while MG_H produces one CH_4 per CO_2 reduced,

$$MG_H = (1 - f)(\Delta CH_4). \quad (7)$$

Total methanogenesis (MG; equation (3)) is the sum of MG_A and MG_H.

[26] Modeled $\sum$C production was then compared with measured $\sum$C production from the control and salinity-amended flow-through reactors. An f value of 0 (i.e., H_2 is the only electron donor for MG) resulted in modeled net $\sum$C that did not agree with measured values, and an f value of 1.0 produced $\sum$C that were too high (Figure 6). Modeled $\sum$C production matched the measured $\sum$C production reasonably well when an f value of 0.5 was used in the control reactors (Figure 6). Modeled $\sum$C in the salinity-amended reactors, using an f of 0.5, matched measured $\sum$C production from about day 12 on, but did not adequately estimate $\sum$C production during the initial period of salinity increase (Figure 6).

[27] Changes in both Fe^{2+} production (Figure 2) and SO_4^{2-} consumption (Figure 3) during the initial salinity breakthrough may have been due to inorganic reactions or errors in calculation (see section 4) rather than changes in microbial respiration. $\sum$C production estimated without contributions of FeR, SR or both FeR and SR were estimated (Figure 6). When $\sum$C production was estimated without FeR (Model minus FeR, Figure 6), modeled DIC production was too high during the salinity breakthrough. $\sum$C modeled without SR (Model minus SR) matched measured $\sum$C production rates quite well until day 11, after which measured $\sum$C production became larger than modeled estimates in the absence of SR. Modeled $\sum$C production without both FeR and SR (model minus SR and FeR, Figure 6) underestimated measured $\sum$C production during the salinity breakthrough. SR was therefore estimated to remain at levels measured in the control sediment until day 11 (see below for further discussion).

[28] The contribution of each terminal electron accepting process (TEAP) to the total mineralization of organic matter was estimated in the control and salinity-amended reactors using results from the models of $\sum$C production (Figure 6). The total organic matter mineralization, estimated from the sum of DIC and CH_4 production ($\sum$C; Figure 7, top) and the fraction of each TEAP, on a per carbon basis, was then determined using an f of 0.5 and model-SR until day 11 in the salinity-amended reactors (Figure 6). In the control reactors, the importance of the terminal electron accepting

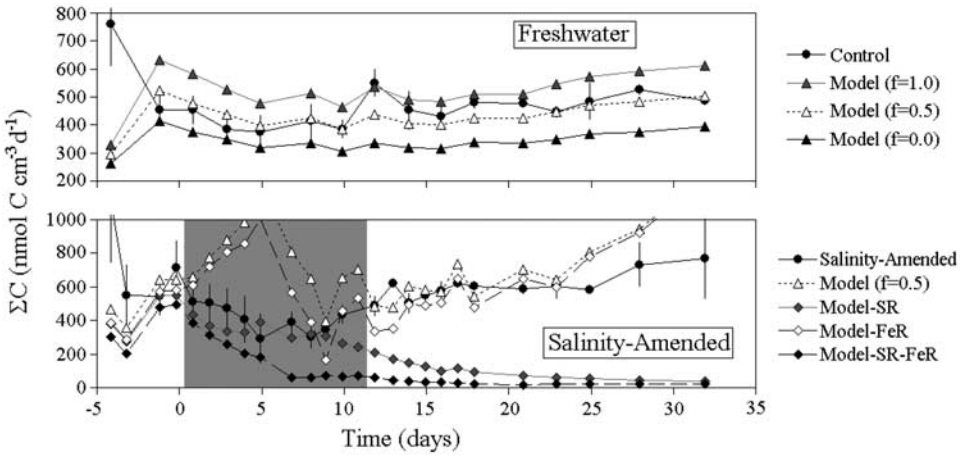

Figure 6. Measured (mean ± standard deviation; n = 6 for day −5 to day 8; n = 4 for day 9 to day 16; n = 2 for day 17 to day 35) and modeled rates of dissolved inorganic carbon (DIC) production in (top) control flow-through reactors (with estimates calculated using different fractions (f) of methanogenesis from organic matter) and (bottom) salinity-amended reactors (including estimates without FeR or SR). The shaded area in the salinity-amended reactors denotes the period for which SR appears to be overestimated. See text for further description.

processes was relatively constant over time and was dominated by MG (62%). SR accounted for 18% of organic carbon oxidation, and contributions of DNF and FeR were similar at about 10% each (Figure 7). The importance of FeR declined to about 5% at the end of the experiment (Figure 7).

[29] In the salinity-amended reactors, organic matter oxidation shifted from MG dominated to SR dominated, with greater than 95% of organic matter oxidized by SO_4^{2-} at the end of the experiment (Figure 7). Carbon flow through DNF dropped to negligible levels during the salinity breakthrough, as did MG by complete breakthrough of 10‰ seawater. FeR appeared to peak in the middle of the salinity breakthrough, accounting for up to 60% of the total organic carbon mineralized for a short period of time (~4 days). SR became the dominant process (>50% organic carbon oxidized) 12 days after initial salinity intrusion (Figure 7).

4. Discussion

[30] Salinity increases in tidal freshwater sediments of the Altamaha River resulted in changes in the concentrations of carbon, nitrogen, phosphorus, silica, iron, and sulfur exiting salinity-amended flow-through reactors (Figures 2–3). These changes resulted from both abiotic geochemical reactions associated with the higher ionic strength of the pore water, as well as shifts in pathways of microbial organic matter mineralization.

[31] Changes in SiO_3^{2-}, NH_4^+ and HPO_4^{2-} concentrations were likely driven largely by the increasing ionic strength of pore water rather than by microbial processes. The presence of cations in solution promotes the hydrolysis of Si-O bonds and the dissolution of quartz minerals [*Dove*, 1999]. Concentrations of SiO_3^{2-} in the water exiting the salinity-amended reactors increased shortly after initial salinity intrusion and remained elevated (Figure 2), indicating enhanced dissolution rates of silica minerals due to salinity intrusion was not a transient process, at least on the timescale of this experiment.

[32] Concentrations of NH_4^+ and HPO_4^{2-} were several orders of magnitude higher in the sediment pore water at the beginning of the experiment (Figure 1) than in the inflow water (Table 2). Although the volume of the flow-through reactors was replaced about twice per day, NH_4^+ and HPO_4^{2-} concentrations exiting the reactors exceeded inflow concentrations for the duration of the experiment (Figure 2), likely due to exchange of adsorbed ions, mineral dissolution, and organic N and P mineralization. For instance, about 40% of the total NH_4^+ export from the freshwater reactors (2.8 μmol cm^{-3}, Table 3) can be attributed to the loss of exchangeable NH_4^+ from the sediments (Figure 5).

[33] The salinity breakthrough was accompanied by an increase in NH_4^+ and a decrease in HPO_4^{2-} concentrations exiting the salinity-amended reactors (Figure 2). Competition for sediment exchange sites by ions in saline waters [*Seitzinger et al.*, 1991] and ion pairing of NH_4^+ and anions in saline water [*Gardner et al.*, 1991] reduces adsorption of NH_4^+ in saline sediments. Desorption of NH_4^+ is a rapid process, taking only hours to reach equilibrium [*Rosenfeld*, 1979]. Concentrations of NH_4^+ exiting the salinity-amended reactors responded to the initial small increase in salinity (from 0.063 in the AFW to 0.161‰ on the first day of amendment), and adsorbed NH_4^+ was exchanged largely at salinities below about 7‰. There was little difference between NH_4^+ concentrations in the control and salinity-amended reactors on day 10, although the salinity was still increasing (Figure 2). The exchangeable NH_4^+ measurements (Figure 5) indicate that the largest fraction (about 70%) of sediment-sorbed NH_4^+ in the initial Altamaha River was exchangeable at low salinities (10‰ exchangeable). Concentrations of 10‰ exchangeable and total exchangeable NH_4^+ were significantly lower in the salinity-amended reactors as early as day 9, and remained lower for the duration of the experiment (Figure 5). Therefore the majority of NH_4^+ desorption from sediments in the Altamaha

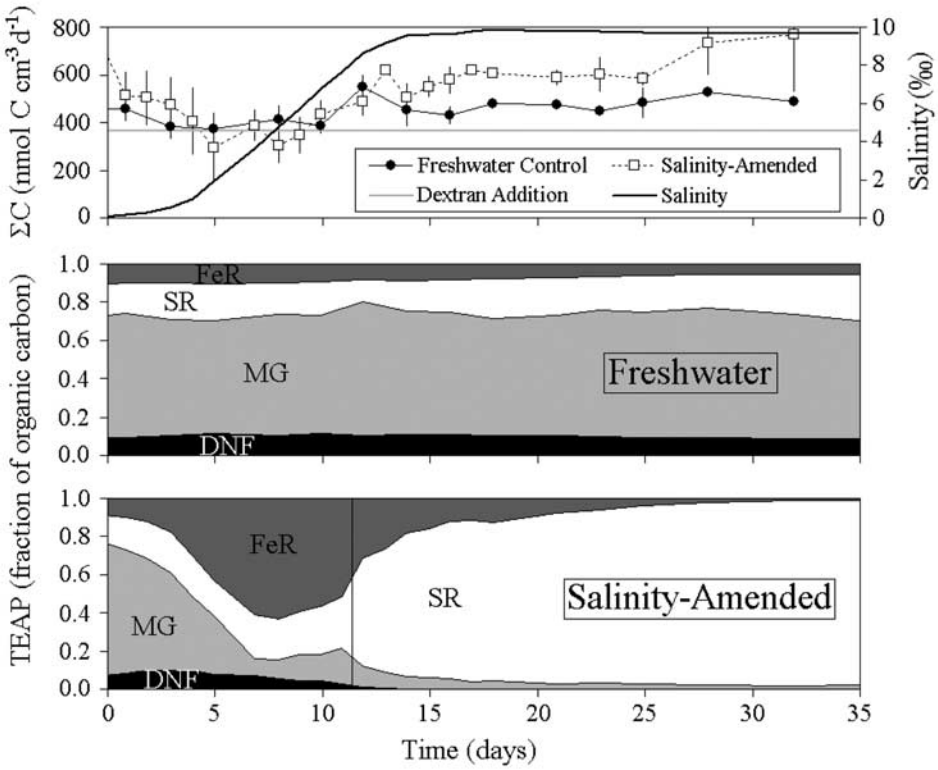

Figure 7. (top) $\sum$C production (sum of DIC and CH_4 production, mean ± standard deviation; n = 6 for day −5 to day 8; n = 4 for day 9 to day 16; n = 2 for day 17 to day 35) in the control and salinity-amended reactors and salinity in the salinity-amended reactors. The dashed line indicates the amount of the dextran polysaccharide added to both control and salinity-amended reactors (nmol C cm^{-3} d^{-1}). Estimated contribution of denitrification (DNF), methanogenesis (MG), sulfate reduction (SR) and iron reduction (FeR) terminal electron accepting processes to total organic carbon oxidation in (middle) control and (bottom) salinity-amended flow-through reactors. The period for which SR was estimated to remain constant in the salinity-amended reactors is indicated by vertical line.

River would occur during the initial intrusion of saline water. Other coastal sediments, however, might release NH_4^+ for a longer period of time following salinity intrusion if they contain larger fractions of NH_4^+ more tightly bound to the sediment matrix [*Morin and Morse*, 1999].

[34] The decrease in HPO_4^{2-} concentrations during the salinity breakthrough was unexpected. As with NH_4^+, adsorption and desorption of HPO_4^{2-} in sediments can control pore water concentrations of HPO_4^{2-} [*Froelich et al.*, 1982; *Sundareshwar and Morris*, 1999], and increasing ionic strength would be expected to desorb exchangeable HPO_4^{2-}. However, HPO_4^{2-} sorption is closely coupled with Fe and aluminum geochemistry in sediments [*Froelich et al.*, 1982; *Sundareshwar and Morris*, 1999]. Potential changes in Fe-oxide surface area (see below) along with increased P mineral precipitation may have lowered HPO_4^{2-} concentrations during the salinity ramp. Following the initial decrease in HPO_4^{2-} concentrations during the salinity breakthrough, HPO_4^{2-} concentrations increased in the salinity-amended reactors (Figure 2) suggesting that HPO_4^{2-} was largely controlled by mineral solubility. However, total HPO_4^{2-} export (Table 3) was about equal to the total inorganic P pool in these sediments, and more than 10% of the total P pool (Table 4). Although variation between samples resulted in no significant differences in any of the P fractions, it appears that mineralization of organic P and subsequent equilibration with the mineral phases in these sediments is the only mechanism by which the measured P export could have been sustained. Changes in sediment P geochemistry following salinity intrusion warrant further study.

[35] The decrease in pH during the salinity breakthrough (Figure 2) is likely due to surface chemistry and ion exchange between the sediments and flushing fluid; decreased pH following salinity increases has been observed by others [*Mahrous et al.*, 1983; *Lu et al.*, 2004]. As the ionic strength of the solution permeating the sediments increases, protons bound to negatively charged sediments are replaced by Na^+ and other ions, decreasing the pH of the pore water.

[36] Estimated rates of microbial activity were significantly different between the control and salinity-amended reactors. Rates of denitrification (DNF) in the reactors (Figure 7) were controlled solely by concentrations of available NO_x, as NO_x was below detection in the water exiting either the control or salinity-amended reactors at all time points. There is some evidence that denitrifying bacteria are inhibited by changes in salinity, especially when freshwater sediments are exposed to saline water, and by HS^- produced by sulfate reducers in marine

systems [*Rysgaard et al.*, 1999; *Mondrup*, 1999; *An and Gardner*, 2002]. N_2O concentrations were low (<0.1 μM) and did not change during salinity intrusion (data not shown). Some fraction of the NO_3^- entering the flow-through reactors may have been converted to NH_4^+ via dissimilatory nitrate reduction to ammonium (DNRA) rather than to N_2 gas by denitrification. However, we were unable to quantify this process because all of the NO_x entering the reactors was consumed and more NH_4^+ exited the reactors than could be accounted for by NO_x reduction.

[37] Methanogenesis dominated the mineralization of organic matter in the freshwater sediments, and estimates from the $\sum$C model indicate that greater than 60% of total carbon was produced by methanogenesis (Figure 7). Concentrations of CH_4 and rates of MG dropped soon after salinity intrusion (Figures 2 and 7). Changes in salinity [*Mishra et al.*, 2003; *Pattnaik et al.*, 2000], competition between methanogens and Fe reducers [*Roden and Wetzel*, 1996] or SO_4^{2-} reducers [*Capone and Kiene*, 1988; *Mishra et al.*, 2003] for substrates, and inhibition of methanogens by HS^- produced by sulfate reduction [*Visser et al.*, 1993; *O'Flaherty et al.*, 1998] can all decrease CH_4 production in sediments. Owing to these inhibitory effects on methanogenesis, rates of CH_4 production and emission from saline sediments are often lower than those observed in freshwater sediments [*Bartlett et al.*, 1987; *Capone and Kiene*, 1988].

[38] It is possible that the anaerobic oxidation of methane (AOM) coupled to SR increased following salinity intrusion, in conjunction with the increased availability of SO_4^{2-} [*Zehnder and Brock*, 1980]. However, the $\sum$C model does not support the production of DIC coupled solely, or even largely, to the consumption of SO_4^{2-} via AOM. Rather, the increased substrate availability and higher energy yields of organic carbon oxidation coupled to the reduction of Fe(III)-oxides and SO_4^{2-} suggest that MG was out-competed by alternate microbial pathways. Thus the lower CH_4 exiting the salinity-amended reactors was likely due to decreased rates of methanogenesis rather than increased rates of AOM. The reduction in CH_4 concentrations in salinity-amended reactors was significant on day 5, corresponding to salinities of less than 2‰, and nearly complete by day 7 (Figures 2 and 7). Even small changes in salinity associated with upriver migration of the freshwater-seawater mixing zone are therefore likely to shift the dominant pathway of organic matter mineralization away from methanogenesis.

[39] We suspect that the apparent consumption of SO_4^{2-} during the initial salinity breakthrough reflects an error in the SO_4^{2-} consumption calculation (equation (1)) due to variable transport of Na^+ and SO_4^{2-} ions through the flow-through reactors during this period. A similar calculation made using Cl^- rather than Na^+ to calculate SO_4^{2-} consumption yielded even greater estimates of SO_4^{2-} consumption. SO_4^{2-} sorption in soils, mainly to aluminum and Fe-oxyhydroxides, is inversely related to pH [*Nodvin et al.*, 1986]. Although usually a minor process at pH > 5, some SO_4^{2-} sorption does still occur at higher pHs [*Camps Arbestain et al.*, 1999]. Retardation of SO_4^{2-} relative to Na^+ in the flow-through reactors during the initial salinity breakthrough (Figure 3), perhaps enhanced by the lower pH during this period (Figure 2), may have resulted in apparent ΔSO_4^{2-} (equation (1); Figure 3) that was not related to microbial sulfate consumption. This is supported by results from the $\sum$C model, in which modeled $\sum$C production was substantially overestimated unless SR was removed during the 10 days following salinity intrusion (Figure 6). Furthermore, it is unlikely that rates of SR in the salinity-amended reactors increased by an order of magnitude above the control rates in 5 days only to decrease to near control rates on day 10 (Figure 3). Thus we suspect that the majority of apparent ΔSO_4^{2-} through day 10 was the result of variable SO_4^{2-} relative to Na^+ transport, and therefore rates of SR were estimated to remain at levels observed in control reactors during this time (shaded area in Figure 6).

[40] Despite the uncertainty in estimating rates of SR during the initial 10 days of salinity-intrusion, SR clearly became the dominant terminal metabolic pathway 12 days after the initiation of salinity-intrusion (Figure 7). Although not often the dominant pathway of organic matter oxidation in freshwater sediments, SO_4^{2-} reduction does occur in freshwater systems [*Holmer and Storkholm*, 2001]. The decrease in SO_4^{2-}/Cl^- ratios in the Altamaha River sediment (Figure 1) suggests that the 3- to 5-cm depth was a zone of active SR and it appears that the existing freshwater sulfate reducing community was able to adapt relatively quickly to increased ionic strength and SO_4^{2-} concentrations.

[41] Concentrations of dithionite reducible Fe [*Poulton and Canfield*, 2005] were high in these sediments (Table 4), but the majority of the Fe(III)-oxides present were apparently not bioavailable at the start of the experiment or in freshwater control reactors (Table 4). Rates of FeR accounted for less than 10% of overall organic matter mineralization in the freshwater controls, FeR declined in importance throughout the experiment (Figure 7), and reducible Fe(III)-oxide concentrations did not change significantly during the experiment (Table 4). *Roden and Wetzel* [1996] found that FeR consumed more than 50% of reducible Fe(III)-oxides within two weeks in freshwater wetland sediments containing Fe(III)-oxide concentrations similar to those observed in the Altamaha River sediments (Table 4). However, sediments often contain a heterogeneous mixture of Fe(III)-oxides with a range of reactivities [*Lovley*, 1991]. The reactivity of metal oxides in sediments is controlled by many factors, including the composition of the oxide, the available metal oxide surface area, sorption of inorganic and organic species on the metal oxide surface, temperature, and the pH and ionic strength of the pore water [*Brown et al.*, 1999; *Roden and Urrutia*, 2002]. The low rates of measured FeR despite high concentrations of Fe(III)-oxides in the freshwater control reactors suggests that these Fe(III)-oxides were either highly crystalline and/or that FeR bacterial access to the Fe(III)-oxide surface was limited.

[42] Fe^{2+} can coat Fe(III)-oxide surfaces and bind to FeR bacteria, inhibiting Fe(III)-oxide reduction by Fe-reducers [*Roden and Urrutia*, 2002]. Rinsing sorbed Fe^{2+} from previously microbially reduced crystalline Fe(III)-oxide (goethite) with a slightly acidic solution can stimulate Fe(III)-oxide reduction [*Roden and Zachara*, 1996]. The decreased pH and increased ionic strength of the pore water during salinity intrusion (Figure 2) may have desorbed Fe^{2+} bound to the Fe(III)-oxide surfaces in these sediments in a

similar manner. The increase in Fe^{2+} concentrations during the salinity intrusion (Figure 2), however, was not due to simple desorption of Fe^{2+} adsorbed to sediment particles. The exchangeable Fe^{2+} content of these sediments was low (<0.5 μmol cm^{-3}; Table 4) and, even if this entire pool dissolved in a single day, it would account for only a change of about 300 μM, which is less Fe^{2+} than was measured exiting the reactors (Figure 2). Though some portion of the measured Fe^{2+} exiting the reactors may have been desorbed from the sediments, the majority (~10 μmol cm^{-3}) appears to have been derived from the microbial reduction of Fe(III)-oxides (Tables 3 and 4).

[43] Owing to the heterogeneity of Fe(III)-oxides in natural sediments [*Lovley*, 1991], the stoichiometry of Fe^{2+} to DIC production may deviate significantly from 4, leading to errors in estimates of FeR using the $\sum$C model. While the magnitude of the estimated FeR may not be well constrained, the modeled $\sum$C production suggests that microbial FeR is required to produce the measured $\sum$C exiting the salinity-amended reactors during the salinity ramp (Figure 6). We therefore hypothesize that salinity intrusion, by increasing the ionic strength and decreasing the pH of the pore water, increased the available surface area of the Fe(III)-oxide pool in these sediments and stimulated microbial FeR during a brief interval.

[44] The labile pool of sediment Fe(III)-oxides that fueled elevated FeR appeared to be rapidly consumed during the initial salinity intrusion because rates of FeR slowed considerably after day 7. Even though reducible Fe(III)-oxide concentrations declined significantly in the salinity-amended reactors, relatively high concentrations (about 50 μmol cm^{-3}) were present at the end of the experiment (Table 4). pH in the salinity-amended reactors increased to levels similar to those in the control reactors after 20 days, and Fe^{2+} concentrations exiting the salinity-amended reactors decreased to levels similar to the controls shortly thereafter (Figure 2). This suggests that the remaining Fe(III)-oxides were unavailable to iron reducers and this may have been caused by sorption of Fe^{2+} to Fe(III)-oxide surfaces [*Roden and Urrutia*, 2002]. Alternatively, precipitation of Fe^{2+} with HS^- produced from SR [*Berner*, 1970] may have resulted in lower concentrations of Fe^{2+} exiting the salinity-amended reactors, which would have underestimated FeR during this period. However, the $\sum$C model would have underestimated terminal carbon production rates if the estimates of FeR were too low, so we suspect that the remaining Fe(III)-oxides were not bioavailable.

[45] Although the pathways of microbial organic matter mineralization are not well constrained during the initial 10 days of salinity intrusion (Figure 6 and 7), this uncertainty is largely a question of the balance between FeR and SR. Rates of MG clearly drop, and DIC is produced by alternate microbial pathways following salinity intrusion (Figures 2 and 7). FeR may have been somewhat overestimated but, if so, rates of SR were concomitantly underestimated. Further, some bacteria are able to reduce both Fe(III)-oxides and SO_4^{2-} [*Lovley et al.*, 1993], such that the shift from FeR to SR may represent a shift in metabolic pathway somewhat independent of a shift in microbial population. Additional work addressing changes in the microbial community at the molecular level following salinity intrusion is in progress.

[46] Total organic matter mineralization appeared to increase following salinity intrusion. $\sum$C production was significantly ($p < 0.05$) higher in the salinity-amended reactors from day 15 on (Figure 7). Increasing ionic strength may have leached labile dissolved organic carbon from sediments (in a manner similar to NH_4^+ desorption) that was then available for microbial utilization. However, DOC and DON concentrations did not change following salinity intrusion (Figure 2), meaning that the leached DOC and DON were rapidly consumed. Further, the increase in $\sum$C production is largely measured toward the end of the salinity breakthrough, and appears to largely reflect an increase in SR (Figure 7). The higher thermodynamic yield of SR as compared to MG [*Stumm and Morgan*, 1996] and the shift in dominance to SR following salinity intrusion suggests that SO_4^{2-} reducers were able to take advantage of in situ organic matter that was not available to methanogens or that they outcompeted the methanogens and iron reducers for carbon substrates that became available during this period.

[47] Pathways of microbial organic matter mineralization were altered dramatically and relatively rapidly following salinity intrusion. MG dominated oxidation of organic matter in freshwater sediments (>60%), with SR (18%), DNF (10%) and FeR (5–10%) further contributing to organic matter mineralization and terminal carbon production (Figure 7). Following salinity-intrusion, microbial pathways of organic matter mineralization shifted initially from MG to FeR (Figure 7), apparently owing to increased availability of sediment Fe(III)-oxides (Table 4 and Figure 4). This was followed by a transition to SR, which became the dominant (>50%) organic matter mineralization pathway within 2 weeks, and SR accounted for greater than 95% of terminal metabolism after 4 weeks (Figure 7).

[48] Overall export of NH_4^+, HPO_4^{2-}, SiO_3^{2-}, Fe^{2+}, CH_4 and $\sum$C from freshwater and salinity impacted sediments were estimated for the 35 days during and following salinity intrusion (Table 3). Export of nutrients (NH_4^+, HPO_4^{2-}, SiO_3^{2-}) was 20 to 40% higher from salinity-amended sediments than from freshwater sediments (Table 3). Despite the drop in HPO_4^{2-} concentrations during the initial salinity intrusion (Figure 2), total HPO_4^{2-} flux from these sediments was higher following salinity intrusion (Table 3). The salinity-driven desorption of NH_4^+ and enhancement of SiO_3^{2-} and HPO_4^{2-} associated mineral dissolution may be sources of these nutrients to coastal waters during up-river salinity intrusion. Excess loading of nutrients has resulted in the eutrophication of many coastal waters [*Nixon et al.*, 1996; *Howarth et al.*, 1996; *Vitousek et al.*, 1997; *Paerl et al.*, 1998], and salinity intrusion may provide yet another mechanism of nutrient supply to fuel excess productivity in the coastal zone. It is interesting to note that the timing of salinity intrusion is likely to coincide with lowest rates of nutrient delivery from the watershed (during low river discharge) amplifying the potential effects in coastal waters.

[49] Lower rates of methanogenesis (Figure 7) resulted in decreased CH_4 export from salinity-impacted sediments (Table 3). The inhibition of methanogenesis following salinity intrusion would reduce emissions of this greenhouse gas to the atmosphere, although owing to the limited geographical extent of salinity intrusion, this reduction would likely be minor on a global scale. Mineralization of

in situ sediment organic matter more than doubled following salinity intrusion (Table 3). Lower CH_4 emissions would then be at least partially offset by lower organic matter burial rates and higher CO_2 release from salinity intrusion impacted sediments due to the ability of sulfate reducers to more efficiently oxidize sediment organic carbon.

[50] **Acknowledgments.** We thank M. Erickson and W. Porubsky for assistance in the field and laboratory, J. Edmonds and M. Moran for discussion of the experimental design, and two anonymous reviewers and the Associate Editor for providing comments that improved the manuscript. This research was supported by the National Science Foundation's Georgia Coastal Ecosystems Long Term Ecological Research Program (OCE 99-82133).

References

An, S., and W. S. Gardner (2002), Dissimilatory nitrate reduction to ammonium (DNRA) as a nitrogen link, versus denitrification as a sink in a shallow estuary (Lagune Madre/Baffin Bay, Texas), *Mar. Ecol. Prog. Ser.*, *237*, 41–50.

Armstrong, J. (1979), Application of the formaldoxime colorimetric method for the determination of manganese in the pore water of anoxic estuarine sediments, *Estuaries*, *3*, 198–201.

Bartlett, K. B., D. S. Bartlett, R. C. Harriss, and D. I. Sebacher (1987), Methane emissions along a salt-marsh salinity gradient, *Biogeochemistry*, *4*, 183–202.

Berner, R. A. (1970), Sedimentary pyrite formation, *Am. J. Sci.*, *268*, 1–23.

Blomqvist, S., G. Anneli, and R. Elmgren (2004), Why the limiting nutrient differs between temperate coastal seas and freshwater lakes: A matter of salt, *Limnol. Oceanogr.*, *49*, 2236–2241.

Brown, G. E., et al. (1999), Metal oxide surfaces and their interactions with aqueous solutions and microbial organisms, *Chem. Rev.*, *99*, 77–174.

Brüchert, V., and C. Arnosti (2003), Anaerobic carbon transformation: Experimental studies with flow-through cells, *Mar. Chem.*, *80*, 171–183.

Camps Arbestain, M. C., M. E. Barreal, and F. Macías (1999), Relating sulfate sorption in forest soils to lithological classes, as defined to calculate critical loads of acidity, *Sci. Total Environ.*, *241*, 181–195.

Capone, D. G., and R. P. Kiene (1988), Comparison of microbial dynamics in marine and fresh-water sediments—Contrasts in anaerobic carbon catabolism, *Limnol. Oceanogr.*, *33*, 725–749.

Caraco, N. F., J. J. Cole, and G. E. Likens (1989), Evidence for sulfate-controlled phosphorus release from sediments of aquatic systems, *Nature*, *341*, 316–318.

Cline, J. D. (1969), Spectrophotometric determination of hydrogen sulfide in natural waters, *Limnol. Oceanogr.*, *14*, 454–458.

Crain, C. M., B. R. Silliman, S. L. Bertness, and M. D. Bertness (2004), Physical and biotic drivers of plant distribution across estuarine salinity gradients, *Ecology*, *85*, 2539–2549.

Dincer, A. R., and F. Kargi (1999), Salt inhibition of nitrification and denitrification in saline wastewater, *Environ. Technol.*, *20*, 1147–1153.

Dove, P. M. (1999), The dissolution kinetics of quartz in aqueous mixed cation solutions, *Geochim. Cosmochim. Acta*, *63*, 3715–3727.

Fanning, J. L. (2003), Water use in Georgia, 2000, and trends, 1950–2000, paper presented at 2003 Georgia Water Resources Conference, Univ. of Ga., Athens.

Froelich, P. N., M. L. Bender, N. A. Luedtke, G. R. Heath, and T. Devries (1982), The marine phosphorus cycle, *Am. J. Sci.*, *282*, 474–511.

Gardner, W. S., S. P. Seitzinger, and J. M. Malczyk (1991), The effects of sea salts on the forms of nitrogen released from estuarine and freshwater sediments: Does ion pairing affect ammonium flux?, *Estuaries*, *14*, 157–166.

Gleick, P. H. (2003), Water use, *Annu. Rev. Environ. Resour.*, *28*, 275–314.

Hamilton, P. (1990), Modeling salinity and circulation for the Columbia River Estuary, *Prog. Oceanogr.*, *25*, 113–156.

Harris, G. P. (1999), Comparison of the biogeochemistry of lakes and estuaries: Ecosystem processes, functional groups, hysteresis effects and interactions between macro- and microbiology, *Mar. Freshwater Res.*, *50*, 791–811.

Holmer, M., and P. Storkholm (2001), Sulphate reduction and sulphur cycling in lake sediments: A review, *Freshwater Biol.*, *46*, 431–451.

Howarth, R. W. (1993), Microbial processes in salt-marsh sediments, in *Aquatic Microbiology: An Ecological Approach*, edited by T. E. Ford, pp. 239–259, Blackwell, Malden, Mass.

Howarth, R. W., et al. (1996), Regional nitrogen budgets and riverine N & P fluxes for the drainages to the North Atlantic Ocean: Natural and human influences, *Biogeochemistry*, *35*, 75–139.

Jørgensen, B. B. (1982), Mineralization of organic-matter in the sea bed—The role of sulfate reduction, *Nature*, *296*, 643–645.

Knowles, N. (2002), Natural and management influences on freshwater inflows and salinity in the San Francisco Estuary at monthly to interannual scales, *Water Resour. Res.*, *38*(12), 1289, doi:10.1029/2001WR000360.

Kupschus, S., and D. Tremain (2001), Associations between fish assemblages and environmental factors in nearshore habitats of a subtropical estuary, *J. Fish Biol.*, *58*, 1383–1403.

Lovley, D. R. (1991), Dissimilatory Fe(III) and Mn(IV) reduction, *Microbiol. Rev.*, *55*, 259–287.

Lovley, D. R., E. E. Roden, E. J. P. Phillips, and J. C. Woodward (1993), Enzymatic iron and uranium reduction by sulfate-reducing bacteria, *Mar. Geol.*, *113*, 41–53.

Lu, S. G., C. Tang, and Z. Rengel (2004), Combined effects of waterlogging and salinity on electrochemistry, water-soluble cations and water dispersible clay in soils with various salinity levels, *Plant Soil*, *264*, 231–245.

Mahrous, F. N., D. S. Mikkelson, and A. A. Hafez (1983), Effect of soil-salinity on the electro-chemical and chemical-kinetics of some plant nutrients in submerged soils, *Plant Soil*, *75*, 455–472.

Mishra, S. R., P. Pattnaik, N. Sethenathan, and T. K. Adhya (2003), Anion-mediated salinity affecting methane production in a flooded alluvial soil, *Geomicrobiol. J.*, *20*, 579–586.

Mondrup, T. (1999), Salinity effects on nitrogen dynamics in estuarine sediment investigated by a plug-flux method, *Biol. Bull.*, *197*, 287–288.

Morin, J., and J. W. Morse (1999), Ammonium release from resuspended sediments in the Laguna Madre estuary, *Mar. Chem.*, *65*, 97–110.

Nixon, S. W., et al. (1996), The fate of nitrogen and phosphorus at the land-sea margin of the North Atlantic Ocean, *Biogeochemistry*, *35*, 141–180.

Nodvin, S. C., C. T. Driscoll, and G. E. Likens (1986), The effect of pH on sulfate adsorption by a forest soil, *Soil Sci.*, *142*, 69–75.

O'Flaherty, V., T. Mahoney, R. O'Kennedy, and E. Colleran (1998), Effect of pH on growth kinetics and sulphide toxicity thresholds of a range of methanogenic, syntrophic and sulphate-reducing bacteria, *Process Biochem.*, *33*, 555–569.

Paerl, H. W., J. L. Pinckney, J. M. Fear, and B. L. Peierls (1998), Ecosystem responses to internal and watershed organic matter loading: Consequences for hypoxia in the eutrophying Neuse River Estuary, North Carolina, USA, *Mar. Ecol. Prog. Ser.*, *166*, 17–25.

Pattnaik, P., S. R. Mishra, K. Bharati, S. R. Mohanty, N. Sethunathan, and T. K. Adhya (2000), Influence of salinity on methanogenesis and associated microflora in tropical rice soils, *Microbiol. Res.*, *155*, 215–220.

Poulton, S. W., and D. E. Canfield (2005), Development of a sequential extraction procedure for iron: Implications for iron partitioning in continentally derived particulates, *Chem. Geol.*, *214*, 209–221.

Roden, E. E., and M. M. Urrutia (2002), Influence of biogenic Fe(II) on bacterial crystalline Fe(III) oxide reduction, *Geomicrobiol. J.*, *19*, 209–251.

Roden, E. E., and R. G. Wetzel (1996), Organic carbon oxidation and suppression of methane production by microbial Fe(III) oxide reduction in vegetated and unvegetated freshwater wetland sediments, *Limnol. Oceanogr.*, *41*, 1733–1748.

Roden, E. E., and J. Z. Zachara (1996), Microbial reduction of crystalline Fe(III) oxides: Influence of oxide surface area and potential for cell growth, *Environ. Sci. Technol.*, *30*, 1618–1628.

Rosenfeld, J. K. (1979), Ammonium adsorption in nearshore anoxic sediments, *Limnol. Oceanogr.*, *24*, 356–364.

Roychoudhury, A. N., E. Vollier, and P. Van Cappellen (1998), A plug flow-through reactor for studying biogeochemical reactions in undisturbed aquatic sediments, *Appl. Geochem.*, *13*, 269–280.

Roychoudhury, A. N., P. Van Cappellen, J. E. Kostka, and E. Vollier (2003), Kinetics of microbially mediated reactions: Dissimilatory sulfate reduction in saltmarsh sediments (Sapelo Island, Georgia, USA), *Estuarine Coastal Shelf Sci.*, *56*, 1001–1010.

Ruttenberg, K. C. (1992), Development of a sequential extraction method for different forms of phosphorus in marine sediment, *Limnol. Oceanogr.*, *37*, 1460–1482.

Rysgaard, S., P. Thastum, T. Dalsgaard, P. B. Christensen, and N. P. Sloth (1999), Effects of salinity on NH_4^+ adsorption capacity, nitrification, and denitrification in Danish estuarine sediments, *Estuaries*, *22*, 21–30.

Ryther, J. H., and W. M. Dunstan (1971), Nitrogen, phosphorus, and eutrophication in coastal marine environment, *Science*, *171*, 1008–1013.

Schindler, D. W. (1977), Evolution of phosphorus limitation in lakes, *Science*, *195*, 260–262.

Seitzinger, S. P., W. S. Gardner, and A. K. Spratt (1991), The effect of salinity on ammonium sorption in aquatic sediments: Implications for benthic nutrient cycling, *Estuaries*, *14*, 167–174.

Smith, S. J., A. M. Thomson, N. J. Rosenberg, R. C. Izaurralde, R. A. Brown, and T. M. L. Wigley (2005), Climate change impacts for the conterminous USA: An integrated assessment: 1. Scenarios and context, *Clim. Change*, *69*, 7–25.

Solorzano, L. (1969), Determination of ammonia in natural waters by the phenol hypochlorite method, *Limnol. Oceanogr.*, *14*, 799–801.

Stookey, L. L. (1970), Ferrozine—A new spectrophotometric reagent for iron, *Anal. Chem.*, *42*, 779–781.

Stumm, W., and J. J. Morgan (1996), *Aquatic Chemistry*, 3rd ed., John Wiley, Hoboken, N. J.

Sundareshwar, P. V., and J. T. Morris (1999), Phosphorus sorption characteristics of intertidal marsh sediments along an estuarine salinity gradient, *Limnol. Oceanogr.*, *44*, 1693–1701.

Visser, A., A. N. Nozhevnikova, and G. Lettinga (1993), Sulfide inhibition of methanogenic activity at various pH levels at 55°C, *J. Chem. Technol. Biotechnol.*, *57*, 9–13.

Vitousek, P. M., H. A. Mooney, J. Lubchenco, and J. M. Melillo (1997), Human domination of Earth's ecosystems, *Science*, *277*, 494–499.

Wigley, T. M. L. (2005), The climate change commitment, *Science*, *307*, 1766–1769.

Wuebbles, D. J., and K. Hayhoe (2002), Atmospheric methane and global change, *Earth Sci. Rev.*, *57*, 177–210.

Zehnder, A. J. B., and T. D. Brock (1980), Anaerobic methane oxidation: Occurrence and ecology, *Appl. Environ. Microbiol.*, *39*, 194–204.

R. E. Dixon and S. B. Joye, Department of Marine Science, University of Georgia, Room 220 Marine Sciences Building, Athens, GA 30602-3636, USA. (raydixon9@hotmail.com; mjoye@uga.edu)

N. B. Weston, Patrick Center for Environmental Research, Academy of Natural Sciences, 1900 Benjamin Franklin Boulevard, Philadelphia, PA 19103, USA. (weston@acnatsci.org)